Chapter 7

Very Long Photon-Lifetimes Achieved by Photonic Atolls

S. Nojima

Additional information is available at the end of the chapter

http://dx.doi.org/10.5772/53435

1. Introduction

It is one of the primary interests in recent nano- and micro-photonics to achieve a strong confinement of light in a small region, because it finds a variety of applications in optical physics and engineering where it is exploited in low-threshold lasers [1], nonlinear optical devices [2], and cavity quantum electrodynamics devices [3]. Extensive efforts have therefore been devoted to developing a cavity that can confine light efficiently—a high-quality optical resonator. The quality of resonators is described here by the photon lifetime τ which is the time that elapses before a photon trapped in the resonator escapes from it, or by the quality factor defined by $Q=\omega\tau$ where ω is the angular frequency of light [4].

In order to achieve high-quality optical resonators, the two directions seem to have been explored so far: one is the use of the extended waves and another is the use of the localized waves. The photonic crystals (PCs) may be the first candidate high-quality resonators, the Q factors for which have been found to be increased by the slowed-down light (the extended waves, or the Bloch waves in this case) near the photonic band edge [5-7]. The typical example for the exploitation of the localized waves can be found in the defect mode that is localized around a disorder in the PC [8-13], which provides more pronounced light-confinement than the band edge modes in the PCs. Although the defect itself generally occupies a very small region, this confinement requires the presence of a large periodic medium around it in order for the defect mode to be sufficiently isolated from its environment. Light can also be localized in the central part of a three-dimensional (3D) fractal structure (Menger sponge) made up of cubes that need not have high Q factors [14]. A single microstructure with a variety of forms [15-19] also creates high-Q modes called whispering gallery modes (WGMs) that occur when the light waves circulate within the microstructure because they undergo total internal reflection at its boundaries. This could be regarded as intermediate between

the two directions mentioned before, since the waves for WGMs are propagating extended waves but confined within the microstructure.

In the context mentioned above, we describe in Sec. 3 an entirely different type of resonator: a closed chain array made up of dielectric microstructures arranged periodically in the background material (e.g., the air). We call it a photonic atoll (PA) resonator because it resembles an atoll in the ocean. This PA resonator is thought to have a prominent function to confine light very strongly for the following reasons: (1) the multiple scattering of light by the periodic quasi-one-dimensional (q1D) array causes a slowing down of extended light-waves and (2) the closed optical path forces a photon once trapped in the array to keep circulating in the loop, both of which would undoubtedly increase the photon lifetime. Factor (1) is the same as the factor responsible for the lifetime enhancement at the band edge of the PCs (see the preceding paragraph) while factor (2) reminds us of the analogy to the ring accelerator for elementary particles. Because of the features mentioned above, this PA structure could also be called a distributed feedback ring-resonator. The above concept was previously [20] applied to the PA resonator of the two-dimensional (2D) circular array consisting of the fifty rods. This resonator was actually found to create an extremely high radiative Q factor of the order of 10^{15} and the resultant very long lifetime of the order of one second for visible light at the modes near the photonic band edges created in this q1D closed PC. The idea of PA was conceived during the investigation of circulating modes in a two-dimensional PC [6, 21] and a microdisk [22], so we believe that the investigation of it and its structure effects will also help us understand the behavior of light in those structures.

Since we have confirmed that the PA structure has a potential to achieve very long lifetimes, our next step of research is to investigate what kind of PA shapes would provide the most efficient optical resonator (Sec. 4). This is because the PA has the degree of freedom that permits it to have an arbitrary loop form: note that the first work (Sec. 3) has focused on a circular PA. In the process of investigations to pursue the optimum PA structure that maximizes the Q value, we observed the remarkable metamorphoses of eigen modes whose degeneracy has been lifted in the modified PAs. This kind of phenomena has so far not been observed in the PA, but it could be considered in the context of the phenomena such as the Stark effect [23] and the Zeeman effect [23] for the electronic energy and the Sagnac effect [22, 24] for the optical energy. This is because the mode splittings in all of these phenomena are caused by some perturbations applied to the system: the Stark effect is caused by the modification of the electronic potential by the electric field, the Zeeman effect by the magnetic field, the Sagnac effect by the mechanical rotation, and our case by the modification of the optical potential by the rearrangement of rods.

Finally, we describe in Sec. 5 the laser actions in the PA resonators with extremely high Q values as an example of their application to a practical optical device. The threshold amplitude gain for laser oscillation is calculated together with the lifetimes. We find that these values are well correlated, in particular that the threshold gain is inversely proportional to the lifetime obtained for the same PA resonators. Although other possible losses of light remain to be considered before this structure is put to practical use, the results obtained here suggest that it would be an excellent structure for confining light. In particular, the fact that

http://dx.doi.org/10.5772/53435

it does not require a large size to achieve a strong light confinement will prove a great advantage over other ways of light confinement when it is incorporated into optical integrated circuits.

2. Theory

2.1. Multiple scattering of light

The analytic multiple-scattering theory is used here to evaluate the light confinement effects. Since the general theory is described in the reports [6, 7], here we briefly outline the framework of the calculation. We consider a 2D array consisting of a finite number N of cylindrical rods (made of material A) with radius d placed at arbitrary points in the background material (material B, usually air). Here we focus on the polarization for which the electric field is parallel to the rod axis (E-polarization). By considering the scattering of the incident plane-wave with the unit amplitude by these rods, we obtain the electric field of the total scattered wave $E^s(\boldsymbol{r})$:

$$E^s(\boldsymbol{r}) = \sum_{n=1}^{N} \sum_{l=-\infty}^{+\infty} b_{nl} H_l^{(1)}(Kr_n) e^{il\theta_n} \equiv \boldsymbol{b} \cdot \boldsymbol{\varphi}(\boldsymbol{r}), \tag{1}$$

where $\boldsymbol{r}$ is the generic coordinate, (r_n, θ_n) is the polar coordinates of the center of the nth rod, and $K = \omega / c$ is the wave number of light in the air. Here, the second equality in Eq. (1) implies the inner product of vectors $\boldsymbol{b} = (b_{nl})$ and $\boldsymbol{\varphi}(\boldsymbol{r}) = \left(H_l^{(1)}(Kr_n) e^{il\theta_n}\right)$ where $H_l^{(1)}(x)$ is the Hankel function [25] of the first kind. Vector $\boldsymbol{b}$ is calculated from the relation $T\boldsymbol{b} = \boldsymbol{q}$, where $\boldsymbol{q}$ is a vector, the size of which is proportional to the amplitude of the incident wave, and T is a matrix:

$$T_{nl,n'l'} = \delta_{nn'}\delta_{ll'} - (1 - \delta_{nn'}) e^{i(l'-l)\phi_{n'n}} H_{l-l'}^{(1)}(KR_{nn'}) s_l, \tag{2}$$

where δ is Kronecker's delta, $R_{nn'}$ is the distance between the centers of the nth and n'th rods, and $\phi_{n'n}$ is the angle that indicates the direction of the n'th rod center as viewed from the nth rod center. Here, s_l is a parameter related to the boundary conditions at the rod surface: see the previous report [6] for its details.

2.2. Modes and lifetimes

To determine the photon lifetime in the photonic atoll, we assume real dielectric constants (i.e., no optical gain) and a complex photon frequency $\omega = \omega' - i\omega''$. Since the frequency dependence of the amplitude of the resonance scattered-wave follows the Breit-Wigner formu-

la [23], the first-order pole of the scattered-wave amplitude gives the complex frequency $\omega_m = \omega'_m - i\omega''_m$ of the resonance mode. Hereafter, we use the subscript m to indicate the specific mode obtained. Since the electric-field amplitude has to diverge at $\omega = \omega_m$ irrespective of position $\boldsymbol{r}$ in $\boldsymbol{\varphi}(\boldsymbol{r})$, this divergence must occur in vector $\boldsymbol{b}$. This implies that the condition $det(T) = 0$ determines the complex frequency ω_m. The photon lifetime of the relevant mode is given by $\tau_m = 1/2\omega''_m$ and the Q factor is given by $\omega'_m \tau_m$.

Here, we refer to the physical meaning of the above method for determining the photon lifetimes. The imaginary part ω''_m of the complex frequency thus determined must be positive since the lifetime is positive. The positive ω''_m means that k''_m is positive due to the relation $\omega_m = ck_m$ in the air, i.e., $\omega'_m - i\omega''_m = c(k'_m - ik''_m)$, where $k_m = k'_m - ik''_m$ is the complex wave number and c is the light velocity (the positive value). Since the 2D scattered wave behaves like $\exp(ik_m r)/\sqrt{r} = \exp(ik'_m r) \cdot \exp(k''_m r)/\sqrt{r}$ at large r, we find that it diverges at the limit of $r \to \infty$ because $k''_m > 0$. This may appear to be unusual, because it is as if light be amplified despite the absence of optical gain in the present physical system. Note, however, that this is true. This actually occurs because the resonance state decays exactly at this resonance frequency to magnify the light intensity outside the PC (not due to gain). In this consideration, the temporal variation of the field should be taken into account at the same time: the light field decreases with the factor $|\exp(-i\omega_m t)| = \exp(-\omega''_m t)$ since $\omega''_m > 0$. The overall behavior of the light field is described by the product of the two factors: the increasing spatial part and the decreasing temporal part. The total light field is thus known to remain unchanged at the simultaneous limits of $r \to \infty$ and $t \to \infty$. We find that the light field energy is conserved during the whole decaying process of the resonance states. This is in marked contrast to the case where the PC has optical gain and therefore the light field energy in the total system is amplified.

2.3. Threshold amplitude-gain for laser oscillation

In the calculation of lasing thresholds [6] in the photonic atoll, we assume that every rod has the same optical amplitude gain K''_a that is the negative imaginary part of the complex wavenumber ($K_a \equiv K'_a - iK''_a$) of light propagating in material A. We introduce the complex dielectric function in order to describe the light amplification in the rod:

$$\varepsilon_a(\omega) = \varepsilon_{a0} - i2c\sqrt{\varepsilon_{a0}}K''_a/\omega, \tag{3}$$

where the photon frequency ω is a real value. Here, ε_{a0} is the dielectric constant of material A in the absence of gain. Taking this complex dielectric function into account in the calculation of the scattered waves, the expansion coefficients $\boldsymbol{b}$ in Eq. (1) can be uniquely determined as $\boldsymbol{b} = T^{-1}\boldsymbol{q}$ when the inverse matrix T^{-1} exists. When there is no incident light wave, we know that $\boldsymbol{q} = 0$, hence $\boldsymbol{b} = 0$, and so we obtain no scattered wave: $E^s(\boldsymbol{r}) = 0$. Note, however,

that there is an exception: if the inverse matrix of T (i.e., T^{-1}) does not exist, we can observe a finite intensity of light even for no light-wave incidence. This is nothing other than a laser oscillation, if it exists. The condition for the nonexistence of T^{-1}, i.e., $\det(T)=0$ can therefore be regarded as the laser oscillation condition. Since matrix T is a complex function of both the photon frequency ω and the amplitude gain K_a'', we can obtain the mode frequency ω_m as well as the threshold amplitude gain K_{am}'' for laser oscillation by searching for the pair of variables (ω, K_a'') at which the determinant for T vanishes. The mode frequency values ω_m thus determined must coincide with those obtained in Sec. 2.2. The easily-oscillating modes have relatively low K_{am}'' values, while those which do not oscillate have higher K_{am}'' values. Therefore, we call the modes the *unlasing modes*, which do not laser-oscillate even under very high K_a'' values that exceed 1.0 (in the units of $2\pi/L$, where L is the period of the rod array: see the first paragraph in Sec. 5 for this normalization).

3. Modes and lifetimes in photonic atolls

The schematic photonic-atoll structure is shown by the inset in Fig. 1. It consists of periodically arranged 50 GaAs rods (with the dielectric constant ε_a=13.18) in the background material air (ε_b=1.0). The typical atoll shape is a perfect circle with the filling factor $f=d/L$ (d: rod radius, L: array period) of 0.45. The expansion up to $|l| \le l_{\max}=12$ was used in Eq. (1) on the basis of the detailed study of its convergence. By numerically solving the equation $\det(T)=0$, we obtain the root ω_m with a sufficient accuracy even for very high Q. Because of the scaling rule that holds in our calculation in a similar manner to in the PCs, the ω and τ values normalized in the units of $2\pi c/L$ and L/c respectively are determined by f (neither d nor L). Hence, the Q factor obtained is independent of the choice of L. Here, we simply use ω instead of ω', the real part of the complex angular frequency, to represent the mode frequency in the description of the results.

3.1. Mode distributions

Figure 1 shows the distribution of optical modes and Q factors for a circular photonic atoll with the filling factor f=0.45. These modes seem to be grouped into several bundles separated by regions with no optical modes. As will be made clearer (see Figs. 2 and 3), the mode bundles and hiatuses seen in Fig. 1 are respectively thought to be photonic bands and band gaps created by the periodic loop array of microstructures, i.e., by the q1D PC.

Let us call these bands #1, #2… etc. from lower to higher frequencies. The #2 and #4 bands are very narrow, but the others are so wide they can be regarded as real bands. These narrow bands are not localized modes, however, because this structure does not contain disorders causing light localization. Actually, these modes have extended (unlocalized) distributions of the light intensity [see Fig. 3(b)]. Although these Q factors have been calcu-

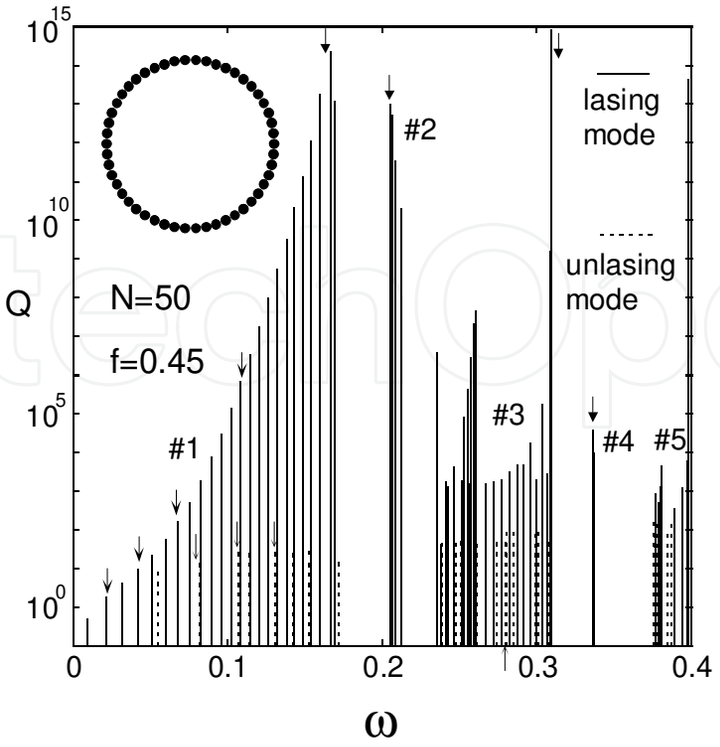

Figure 1. Distribution of optical modes on the frequency axis for a closed circular array of 50 GaAsmicrorods (see the inset). The heights of the columns indicate the values of the *Q* factors for the modes, ω is normalized in the units of $2\pi c / L$, and the filling factor $f = d / L$ (*d*: rod radius, *L*: array period) is 0.45. Here, no optical gain is considered in the calculation of the *Q* factors (see Sec. 2.2). Modes shown by solid and dotted lines respectively indicate those which lase and unlase (see Sec. 2.3 for the definition of *unlase*). See also Fig. 3 for the modes denoted by arrows.

lated assuming no optical gain, another examination assuming optical gain in every rod revealed that these modes can be classified into two types depending on whether they did lase (solid lines) or did not lase even by giving very high optical gains (dotted lines, see also §2.3). As shown in Fig. 1, the *Q* factors (i.e., those obtained assuming no gain) for the lasing modes are very high whereas those for unlasing modes are relatively low (10 to 100). What causes this difference will be clarified later (see Sec. 3.3). In the first band #1, the *Q* factor for lasing modes increases rapidly toward the band edge and reaches a maximum near it. Although the *Q*-factor variation for lasing modes in other bands is more complicated, the *Q* factor there also tends to become higher at the band edges. At the top edge of band #3 (ω_m=0.3097), the *Q* factor reaches the extremely high value of 0.8×10^{15}. This high *Q* would allow light to stay in the photonic atoll for about 1 second, a surprisingly long time for the visible light, if we assume ideal circumstances that let us neglect other losses. Although one may think that these high-*Q* modes have been created fortuitously, we have confirmed that they are always observed at the same band edges in this kind of structure. These results indicate that the atoll structure has a potential to confine light very strongly: its geometry inherently involves the high-*Q* effect.

The significance of the above results can be better understood by comparing them with the results obtained with other resonators. The *Q* factors of modes at the band edge of a 2D PC

with 53 rods are ~ 100 [7]. The Q factors for modes in a photonic atoll, in contrast, are more than 12 orders of magnitude larger ($\sim 10^{15}$) despite the fact that both stem from the extended modes in similar-sized resonators. The high-Q localization also occurs in a defect mode in the PC with lateral Q factors of the order of 10^4 [8, 9], which are still lower than the present Q. This localization occurs around a defect that is sufficiently separated from the outer environment so that the coupling between them is cut off. This implies that the defect has to be surrounded by a considerable volume of the periodic medium (PC). It is actually reported that nearly 400 rods are needed to isolate the defect mode in a PC [8]. The presence of so many rods despite the smallness of the defect would be disadvantageous with regard to incorporating an optical cavity in the PC. The present photonic atoll permits us to obtain much higher Q factors by using a small number of rods with little deterioration of them by the presence of dielectric materials near it. This demonstrates the advantage of this resonator over the defect mode localized in a regular PC. These Q factors are also found to be higher than those for the WGMs in a rod ($\sim 10^{10}$) [17]. Although the present model does not consider the vertical Q that comes to play a certain role in the slab, we find that the photonic atoll greatly strengthens the confinement of light propagating in the 2D space.

3.2. Filling-factor effects

The finding of bands and band gaps has given impetus to the study of filling-factor effects, as is often carried out in the ordinary PCs [26]. Figure 2 shows the variation of the positions of bands (shaded areas) and band gaps (blank areas) as a function of the f value. Here, we focused on bands and band gaps created by lasing modes (solid lines in Fig. 1), because they are verified later to be generated along the rod loop (see Fig. 3). The vertical broken line corresponds to Fig. 1. Let us scan the results from low to high f values. Since $f=0$ implies uniform air (no rods), the mode distribution is continuous (i.e., without bands and band gaps). With increasing f, the closed periodic array structure comes into existence and as a result the continuous free-space dispersion gradually splits into several bands: this occurs at $f<0.1$ (not explicitly shown in Fig. 2). We see that a large band gap is produced between bands #1 and #3. Further increase in f splits band #3 to create a new narrow band #2. This new band remains narrow until f reaches its maximum value. A similar phenomenon occurs in band #5, which splits to form a narrow band #4 around $f=0.4$. The first band gap formed between bands #1 and #3 ($f<0.35$) appears to be maximized at a certain filling factor that is intermediate between 0 and 0.25, because the band gap vanishing at $f=0$ undoubtedly increases for $f>0$ but decreases for $f>0.25$. The existence of an optimum filling factor for the large-gap generation is similar to what is seen in the ordinary PCs [26]. The formation of narrow bands for $f>0.35$ is not well understood, but some modes with nodes produced in the loop-radial direction may be involved in their formation because of the increased rod radius for higher f values. These results substantiates for the first time the creation of photonic bands and band gaps in a q1D looped array structure like the photonic-atoll resonator proposed here.

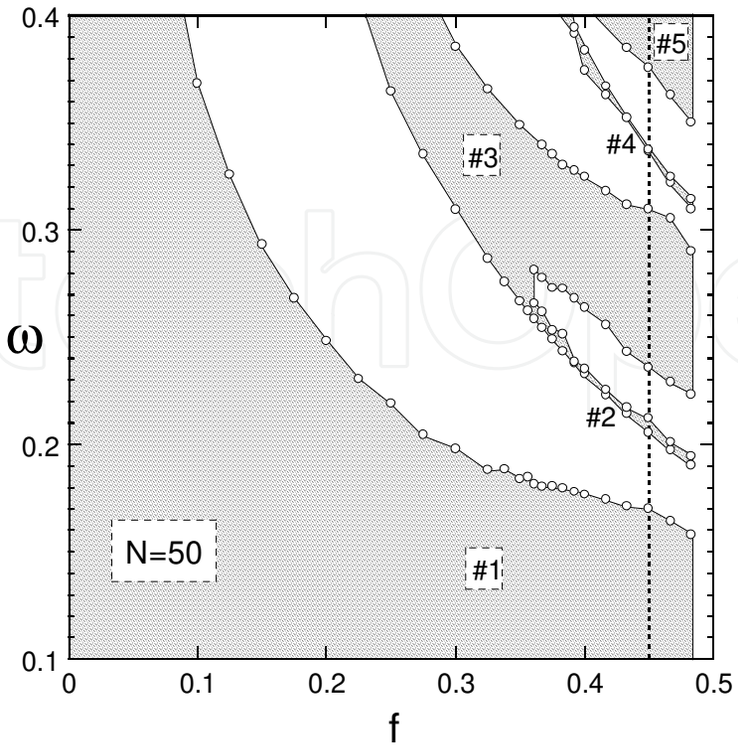

Figure 2. Variation of the bands (shaded areas) and band gaps (blank areas) formed by lasing modes (solid lines in Fig. 1) as a function of rod filling factor *f*. *f* = 0 corresponds to only air (no rods), and *f* = 0.5 corresponds to the configuration in which neighboring rods touch one another.

3.3. Light intensity distributions

In order to clarify what occurs for these modes, we next investigate the field intensity distributions in the photonic atoll. Note again that no gain is assumed for this calculation. We first select several lasing modes from band #1, because the modes in the first band with relatively long wavelengths are expected to provide a variety of clues to the understanding of the fundamental processes of light localization. Figure 3(a) shows the light-intensity distributions for the four lower lasing modes in band #1 (indicated by arrows in Fig. 1). In the colored figures, the intensity increases in the order blue, white, yellow, red, and black. The numerals in the figure are the mode frequency values and from left to right in Fig. 3(a), they respectively correspond to Q factors of 1.7, 9, 150, and 6.6×10^5. Although the light confinement is not very strong for these modes, we can clearly recognize the process in which light comes to be localized along the loop as Q increases. We also find a noticeable variation of the field distributions. First, the lowest-frequency mode (ω_m=0.0216) appears to have two loops and nodes of light waves along the array loop. This implies that the wavelength λ is comparable to the circumference D of the circular loop. If we assume the light propagation along the array loop with a wavenumber vector $\boldsymbol{K} = K\boldsymbol{e}$ ($\boldsymbol{e}$ is the unit vector along it) and a light velocity $v = c/n_{eff}$, this mode gives an effective refractive index n_{eff} of about 0.93. This value is close to the n_{eff} of 1 for air, which is reasonable since most light is leaked into the air

http://dx.doi.org/10.5772/53435

because of the small Q of this mode. The second mode (ω_m=0.0421) appears to have six loops and nodes giving $\lambda \sim D/3$, which leads to $n_{eff} \sim 1.4$. Further increase in the mode frequency enables us to observe distinct light localizations toward the rod array. The modes ω_m=0.0678 and ω_m=0.1086 respectively give wavelengths of $\lambda \sim D/6$ and $\sim D/12$. The similar estimation of n_{eff} leads to respective n_{eff} values of 1.8 and 2.2 for these modes. The gradual increase in the estimated n_{eff} toward $\sqrt{\varepsilon_a}$=3.6 for the rods reconfirms the increased light confinement in the rod array loop. The light confinement along the rod chain may also be construed by the coupling between a WGM mode in a rod and the one in its neighboring rod via their Fano resonances with the outer region [27].

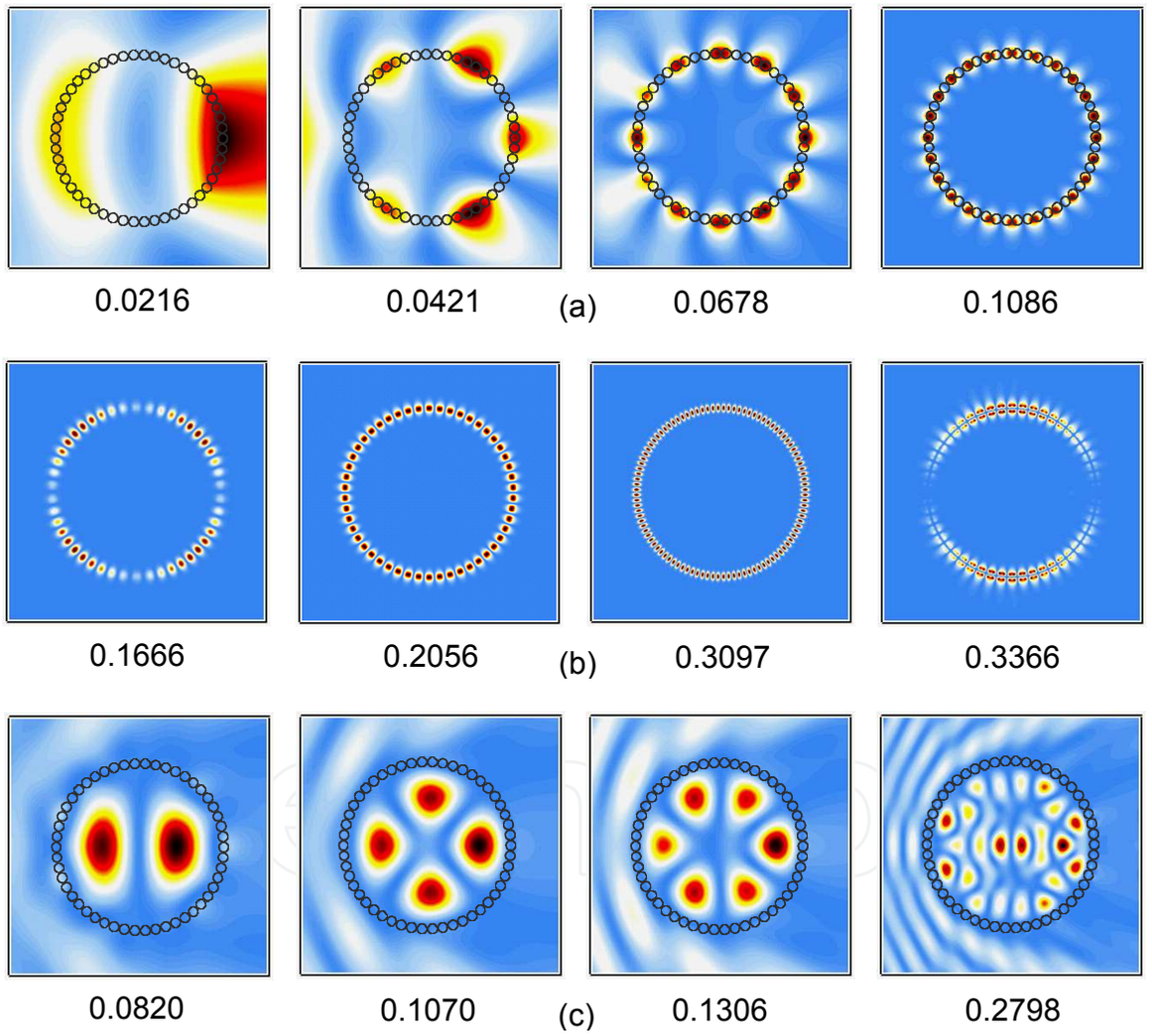

Figure 3. Color) Light intensity distributions for (a) lasing modes in the first band #1, (b) lasing modes with very high *Q*-factors, and (c) unlasing modes (see §2.3 for the definition of *unlasing modes*). Here, note that no optical gain is assumed for the calculation of these intensity distributions. The numeral shown under each figure is the normalized-mode frequency: see Fig. 1, where different symbols of arrows are used to distinguish the modes in Figs. 3(a), (b) and (c). The intensity increases in the following order: blue < white < yellow < red < black. Rod positions are indicated in Figs. 3(a) and 3(c) by black circles but for clarity they are not indicated in Fig. 3(b).

Several examples for the modes with very high Q-factors are shown in Fig. 3(b). These modes are selected as those having the maximum Q factor values in each band from #1 to #4 (see the arrows in Fig. 1). The strong light-confinement for these modes is confirmed by comparing the intensity (i.e., unity) of the incident plane-wave and the maximum light intensity in the rod array: the first three modes (ω_m=0.1666, 0.2056, and 0.3097) all have intensity of the order of 10^{11} and the last one (ω_m=0.3366) the order of 10^5. Note that this intense light is obtained in the array with no optical gain (no gain is assumed here!). It is entirely due to the extremely long photon lifetimes attained by the use of photonic-atoll resonators. Although light is focused on the rod array, its intensity distributions are not easy to construe. Let us focus on the bright regions, which are the loops of light waves. While the contour of bright regions for the mode in band #1 (ω_m=0.1666) is simple, the contour of bright regions for the mode in band #2 (ω_m=0.2056) contains two brightest points (not clearly seen for a small drawing). The mode in band #3 (ω_m=0.3097) has many bright regions (100, or twice the rod number of 50) though its contour is simple. The most extraordinary results are found in the mode in band #4 (ω_m=0.3366), for which the bright region consists of two small units separated in the radial direction of the loop and each small unit has two brightest points. The modes in higher-index bands thus tend to become complicated. This evidently stems from the higher-order Bragg reflections to create these bands, which occur in the q1D closed array.

Shown in Fig. 3(c) are for the modes that never lase even if they have very high gains (the modes shown by dotted lines in Fig. 1). Light for these modes is clearly confined in the inner region of the atoll but not along the rod array. We see an increase in the number of loops and nodes as the mode frequency increases, indicating that they are formed by light trapped in the inner region and reflected at the rod array of the atoll. The observed Q factors (10–100) are small despite the expectations for the WGMs to produce strong light confinement. The above results are reasonable, however, because both inner and outer regions are made from the air and hence the thin array loop does not serve as a solidly made pool for light. We also understand that these modes do not lase because light stays in the region with no gain.

4. Shape effects of photonic atolls

In this section, we assume the PA that consists of 20 GaAs rods (with the dielectric constant ε_a=13.18) in the air (ε_b=1.0). We consider a variety of elliptical PAs created by changing its eccentricity e from 0 to 0.968. For all the PAs studied here, however, the filling factor $f = a/L$ (d: rod radius, L : period) is fixed at 0.45 and the period of the rod chain is assumed to be the same. Moreover, we modify the PA form keeping its circumference fixed in order to facilitate the comparison between the PAs with different eccentricities. The angular frequency ω and the lifetime τ are expressed in the units of $2\pi c/L$ and L/c, respectively. Here, we again simply use ω instead of ω', the real part of the complex angular frequency, to represent the mode frequency in the description of the results.

4.1. Splitting of degenerate modes

Prior to showing the detailed properties of the PAs, we first present the basic results for the optical modes created in the PA. Figure 4 shows the angular frequency ω positions for the

http://dx.doi.org/10.5772/53435

optical modes (denoted as n=0, 1, 2, …, 10 for low to high ω modes), where the height of the columns indicates the lifetime τ of these modes. The thin lines are the results for the circular PA (e=0) shown in the inset. In the limit of the infinite number of rods, these modes get accumulated densely to form the first photonic band of the q1D closed photonic crystal [20] and hence the shaded region in Fig. 4 can be regarded as the first photonic band gap. As shown in Fig. 4, the lifetime becomes longer with the mode frequency that is increasing and approaching the first band edge. Here, let us examine the specific numerical values. We take mode 10 as an example with the dimensionless values $\omega = 0.1691$ and $\tau = 6.30 \times 10^6$, and $L = 0.1 \mu m$ for the periodicity. These values give the actual frequency $\omega / 2\pi = 510\, THz$ (the visible light with wavelength $\lambda = 0.59\, \mu m$) and the actual lifetime $\tau = 2.1\ ns$. The above results demonstrate the presence of the enhanced confinement of light near the band edge [6, 7]. The thick lines indicate the results for an extremely deformed PA (e=0.866), the form of which is also shown in the inset. We see the lifetime remarkably decreased by the use of the elliptical PA, which occurs more pronouncedly for higher modes. The examination of a variety of elliptical PAs showed that any PA modifications caused the decrease in the lifetime. We have to admit that these results for the deformed PAs are discouraging from the viewpoint of the achievement of longer lifetimes. Here, we observe some notable phenomena, however: twin modes are isolated in the vicinity of the circular-PA modes with n=1, 2, …, 9. Note that no twin modes are created for n=0 and 10.

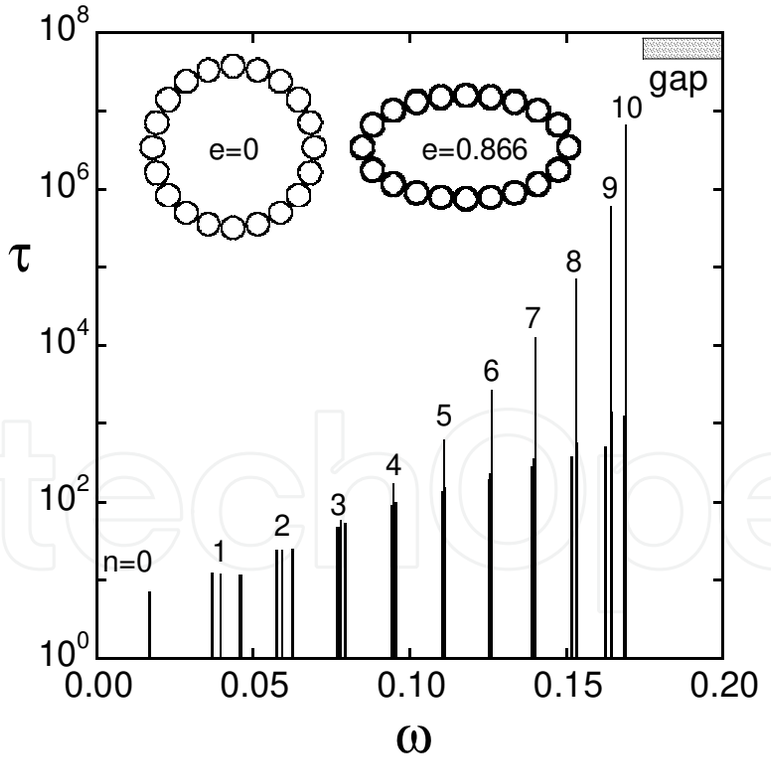

Figure 4. Optical modes distributed on the frequency axis, where the height of the columns indicates the lifetime of these modes. The thin and thick lines are the results for the PAs as shown in the insets: a perfect circle (e=0) and an ellipse (e=0.866), respectively, where e is the eccentricity of the elliptic PA. Here, several thin lines are hidden behind thick lines since the latter are superimposed onto the former. In this paper, the angular frequency $\omega$and the lifetime τ are normalized in the units of $2\pi c / L$ and L / c, respectively, where L is the period of the PA chain.

The similar studies have been carried out for elliptical PAs with a variety of eccentricities. The results are summarized in Fig. 5, which shows the variation of the mode frequency as a function of the eccentricity e (from 0 to 0.968). As clearly shown in Fig. 5, each of modes 1-9 is found to split into two with the increasing eccentricity. Those modes that are increasing and decreasing, respectively, with the growing eccentricity are denoted by open and close circles. While we succeeded in locating almost all split-modes very precisely, we failed in isolating several higher modes (open circles) split for mode 1 at e>0.954. Here, we can read in Fig. 5 what follows. First, the splitting width strongly depends upon the optical mode as well as the PA form. In fact, modes 1, 2, and 9 already exhibit slight but clear splittings even at relatively low e values (e<0.5), while modes 4, 5, and 6 do not split until it reaches a value higher than 0.8. These results will be more clearly displayed later in Fig. 6. Second, we also recognize a strong mode-dependence of the frequency deviation from the original one (e=0). Let us denote the deviations by $\Delta\omega_H \equiv \omega_H - \omega$ and $\Delta\omega_L \equiv \omega - \omega_L$ for the modes shifted in the higher and lower directions, respectively. We can paraphrase the above facts as follows: $\Delta\omega_H > \Delta\omega_L$ for modes 1, 2, 3, and 4, $\Delta\omega_H \simeq \Delta\omega_L$ for modes 5 and 6, and $\Delta\omega_H < \Delta\omega_L$ for modes 7, 8, and 9, when they are compared at a fixed eccentricity. These facts suggest the presence of different mode-splitting mechanisms between the modes near the Γ point, the modes in the middle of the band, and the modes near the band edge. Finally, let us briefly refer to modes 0 and 10. These modes did not split for all the e values studied here. However, noteworthy here is that mode 0 slightly increases while mode 10 decreases to a certain extent, according as the eccentricity grows. This fact again suggests the difference in the behavior between the near-Γ-point modes and the near-band-edge modes.

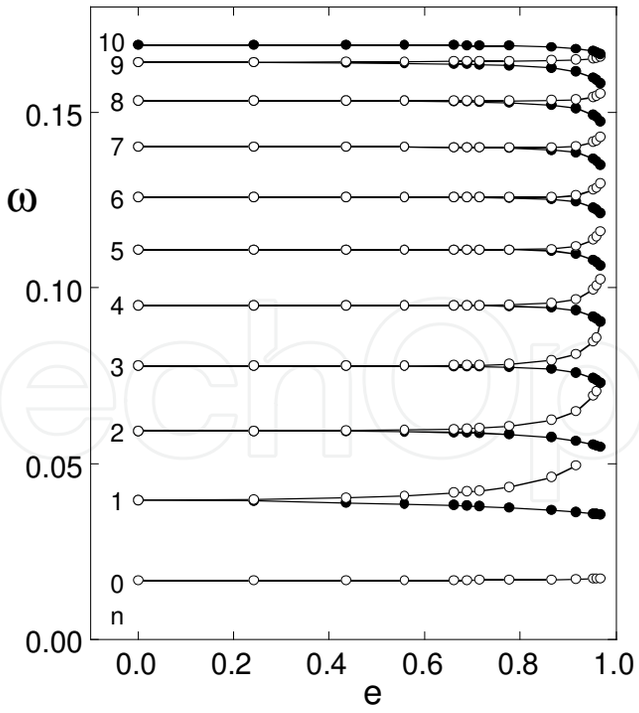

Figure 5. Frequency positions of all modes in the first band as a function of the eccentricity e for the elliptical PA. Here, the upper and lower modes split by the PA modification are denoted by open and closed circles, respectively (except for modes 0 and 10).

http://dx.doi.org/10.5772/53435

Figure 6 shows the mode separation $\Delta\omega \equiv \omega_H - \omega_L$ as a function of the frequency position of the mode, which is evaluated at a variety of the PA eccentricity values. The e value for each curve is given in the caption of Fig. 6. As mentioned before, modes 0 and 10 have no split modes. What is intriguing here is that the separation $\Delta\omega$ is not a monotonic function of the mode frequency: it becomes more prominent as they approach the bottom or the top of the band and moreover exhibits a minimum at the middle of the band. When we look at Fig. 6 precisely, the above phenomena are found to occur more pronouncedly for a slightly deformed PA: see, e.g., the results for e=0.243, in which the ratio of $\Delta\omega$ between mode 1 and mode 5 reaches as high as 1.7×10^5. On the other hand, in the extremely deformed structures, we find no significant mode dependence of $\Delta\omega$ though these modes have larger frequency splittings. This kind of phenomena has not been observed in the finite-sized optical resonators and even in the similar mode-splitting phenomena [22-24] referred to in Sec. 1 either.

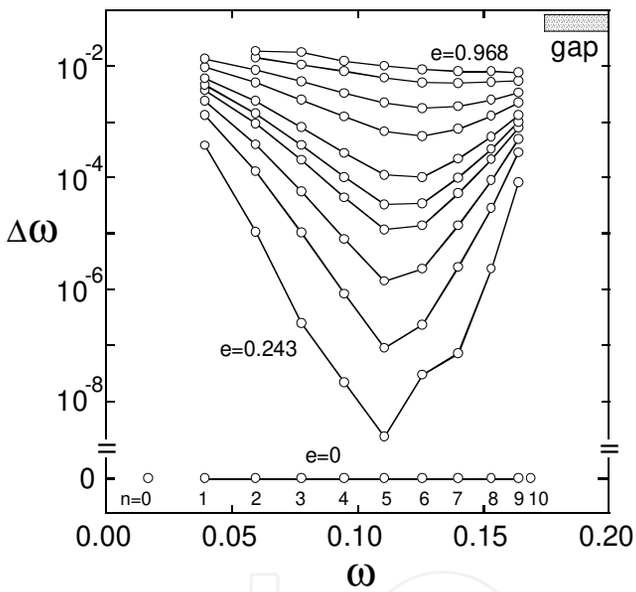

Figure 6. Relations between the split-modes separation $\Delta\omega$ and the mode frequency position for several eccentricity values. Here, the e value ranges from 0, 0.243, 0.436, 0.558, 0.661, 0.714, 0.777, 0.866, 0.916, 0.954, and 0.968, for the curves displayed from bottom to top, respectively.

4.2. Light intensity distributions

The results mentioned in Sec. 4.1 have prompted us to investigate the light field distributions for these modes. Hereafter, we focus on the PA with e=0.866 and modes 2, 5, and 9, which have been selected as the optical modes located near the Γ point, in the middle of the band, and near the band edge, respectively. We denote, in what follows, the higher and lower modes split as nH and nL, respectively, for mode n.

Figure 7 shows the light intensity distributions for (a) mode 2L with θ_i=0 , (b) mode 2L with θ_i=90 , (c) mode 2H with θ_i=0 , and (d) mode 2H with θ_i=90 . Here, θ_i is the incident angle of the plane wave of light. The rod array of the PA is also displayed together with the distributions in Fig. 7. Here, the light intensity increases in the order blue, white, yellow, red, and black. Since our calculation is based on the scattering-theoretic method [6], the incident plane wave is included in the distributions as a matter of course. As shown in Fig. 7, these modes have four nodes and loops along the rod chain of the PA and show the weak light confinement because of their shorter lifetimes (see Fig. 4). We find these modes to be excited by the irradiation of light from any directions including 0 *and* 90 shown in Fig. 7, although the maximum intensity of light excited in the PA somewhat differs depending on the directions of incidence. Since its difference reaches only a few times, however, we may conclude that there is no preference in the irradiation direction for their excitation in this case. This fact presents a great contrast to the band-edge modes as shown later (Fig. 8). Although modes 2H and 2L are thus excited by light with any incidence directions, their light distributions depend entirely on the irradiation direction, as shown in Fig. 7. In addition, the oblique incidence with, e.g., θ_i=45 creates light distributions like those obtained by rotating Figs. 7 (a) and 7(c) by 45 . In other words, their wave functions remain uncertain for the unirradiated PAs. This fact is suggestive of the similarity to the electronic mode in an atom. Once the PA is irradiated by a plane wave of light, however, their wave functions are uniquely determined as follows: the incident wave selects their wave functions in such a manner that it can excite the eigen modes based on the symmetry matching between them. The irradiation direction thus works as the quantization axis in the quantum theory. When we look at Fig. 7 in more detail, we find that most light is focused around the downstream side of the PA chain for mode 2L. For mode 2H, on the other hand, we recognize light staying around the upstream side of the PA chain though some light is still around the downstream side. The massive flow of the incident beam generally tends to cause the light distribution to be more highlighted at the downstream side [20], which could correspond to an energetically more stable state. Taking this circumstance into account, we may come to a reasonable conclusion that modes 2L and 2H, respectively—energetically stable and unstable states—concentrate around the downstream and upstream sides. This is true for all incident angles and all other modes near the Γ point. We thus have made clear the difference between the light fields for the modes—located near the bottom of the band—that are split by the modification of the PA structure.

Next, we display the results for the modes near the band edge as a matter of convenience for explanation. Figure 8 shows the light intensity distributions for (a) mode 9L with θ_i=0 , (b) mode 9L with θ_i=90 , (c) mode 9H with θ_i=0 , and (d) mode 9H with θ_i=90 . As can be seen in Figs. 8(a) and 8(d), these modes have 18 nodes and loops along the rod chain of the PA and exhibit somewhat strong light confinement because of their relatively long lifetimes (see Fig. 4). The most striking feature for these modes is found in the pronounced θ_i-dependence of their excitation. In fact, as clearly shown in Fig. 8, mode 9L is excited by the irradiation

http://dx.doi.org/10.5772/53435

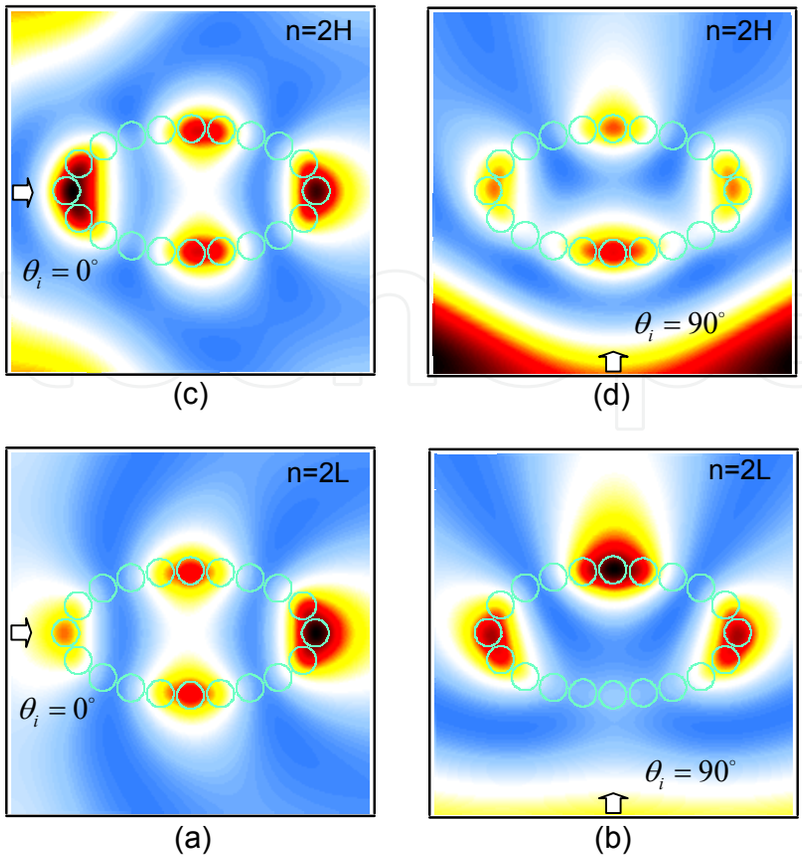

Figure 7. Light intensity distributions for (a) mode 2L with $\theta_i = 0^\circ$, (b) mode 2L with $\theta_i = 90^\circ$, (c) mode 2H with $\theta_i = 0^\circ$, and (d) mode 2H with $\theta_i = 90^\circ$. Here, θ_i is the incident angle of the plane wave of light. The rod array of the PA is also displayed together with the distributions. Here, the light intensity increases in the order blue, white, yellow, red, and black.

with the incident angle 0 whereas it is not by the 90 irradiation. In the similar manner, mode 9H is excited by the irradiation with the incident angle 90 whereas it is not by the 0 irradiation. A very high value of several hundreds is reached for the ratio of the maximum intensity of light confined around the rod array between the incident directions causing (e.g., 90 for mode 9H) and not causing (e.g., 0 for mode 9H) its excitation. These results, when viewed from another point, demonstrate that mode 9H is excited efficiently by the irradiation of light that excites mode 9L less efficiently, and vice versa. The same phenomena are confirmed to occur for all other modes near the band edge for the irradiation from any directions and even in the slightly modified PA ($e = 0.243$). From these results, we speculate that these modes are orthogonal to each other since optical mode can be excited only by the light beam with the same symmetricity as the relevant mode. This fact provides a striking contrast to the modes near Γ point (see Fig. 7), which are excited by the irradiation with any incident directions.

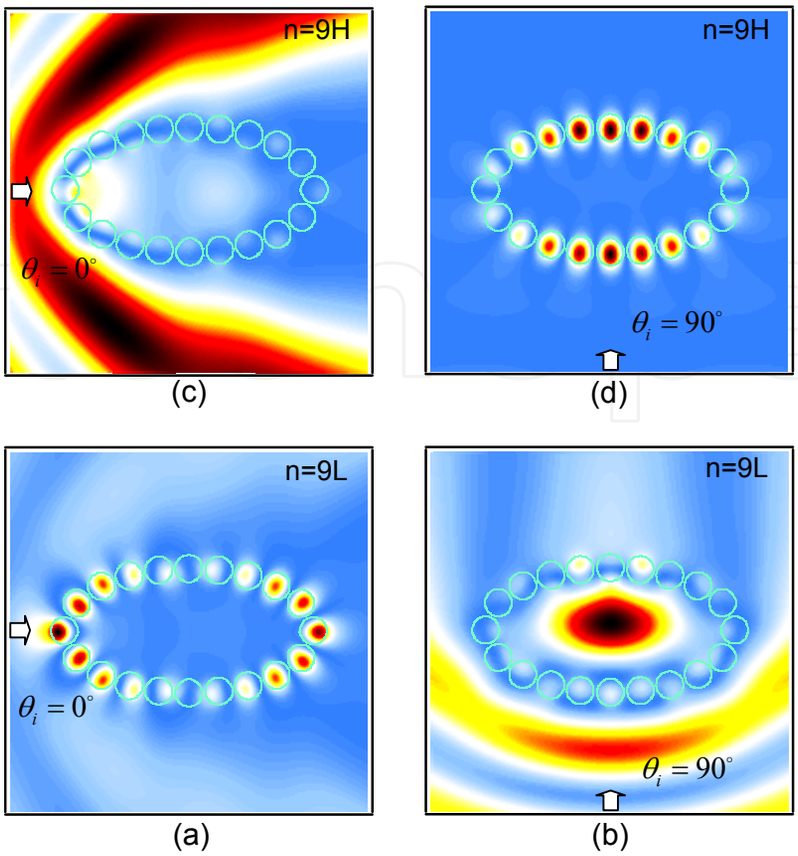

Figure 8. Light intensity distributions for (a) mode 9L with $\theta_i = 0^\circ$, (b) mode 9L with $\theta_i = 90^\circ$, (c) mode 9H with $\theta_i = 0^\circ$, and (d) mode 9H with $\theta_i = 90^\circ$.

Finally, we briefly mention the behavior of the modes in the middle of the band. Figure 9 shows the light intensity distributions for (a) mode 5L with $\theta_i = 0$, (b) mode 5L with $\theta_i = 90$, (c) mode 5H with $\theta_i = 0$, and (d) mode 5H with $\theta_i = 90$. These modes have 10 nodes and loops along the rod chain of the PA. In contrast to modes 2L and 2H mentioned before, these modes have no pronounced concentration of the intensity distribution on the upstream or downstream sides of the PA. Moreover, they exhibit no irradiation-direction dependence of the excitation, which has been detected for modes 9L and 9H. These modes are thus known to have the characteristics that are intermediate between the near-Γ-point modes and the near band-edge modes.

4.3. Discussion

Let us discuss the creation of eigen modes and their splitting by the structural modification of the PA resonator. For this purpose, we simplify the discussion by regarding the closed q1D chain as a closed pure-1D system with the position variable x along the circumference. The periodic boundary condition can be applied to this system exactly for its closed structure, and the Bloch theorem for the L-periodicity of the PA. We thus obtain the optical

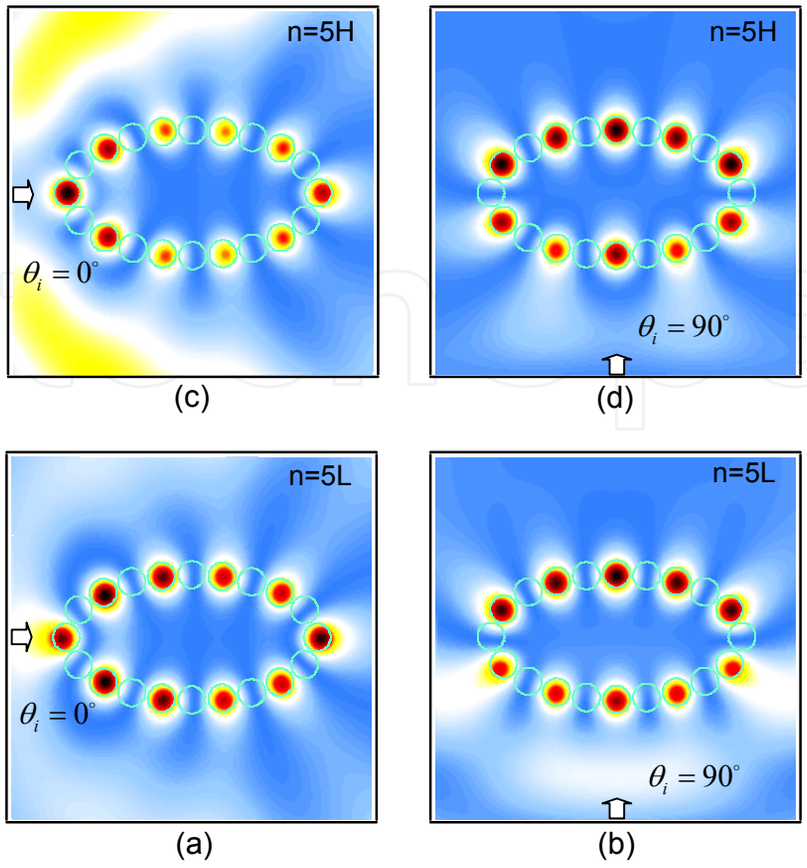

Figure 9. Light intensity distributions for (a) mode 5L with $\theta_i = 0^\circ$, (b) mode 5L with $\theta_i = 90^\circ$, (c) mode 5H with $\theta_i = 0^\circ$, and (d) mode 5H with $\theta_i = 90^\circ$.

modes specified by the wave number $k_n = g(n/20)$ for the wave propagating along the chain with 20 rods, where $g = 2\pi / L$ is the fundamental vector in the reciprocal space. Here, n ranges over –9,…, –1, 0, +1,…, +9, and +10, creating 20 modes. Note that n= –10 is excluded since it is identical to n= +10 in the reciprocal space. The modes with n are thus known to be degenerate with those with $-n$ for n=1, 2,…, 9 and their wave functions are the complex conjugate of each other, which propagate in the opposite directions with the wave numbers $+k_n$ and $-k_n$, respectively. Moreover, we understand that the lowest mode 0 and the band-edge mode 10 are not degenerate: here, we note in passing that the band-edge mode is doubly degenerate for the PA with the odd-numbered rods, e.g., 21 rods.

When we look at Figs. 4-6 together with the above considerations, it is not unusual for modes 0 and 10 to remain single under any perturbations given to the structure because of their nondegeneracy. As for the other modes (n=1, 2,…, 9), it is reasonable to consider that their degeneracy is lifted by the modification of the PA structure. If we apply the group theory to this phenomenon straightforwardly, it may be said that the degeneracy lifting is caused by the reduction of the rotational symmetry in the whole PA structure. Although this is an elementary but important interpretation for these degeneracy-lifting phenomena, we

here refer to another perspective. Under the assumption to regard the PA as a very long closed 1D structure—it is actually possible as mentioned before, the waves propagating in the opposite directions ($+k_n$ and $-k_n$) ought to split their frequency only in the presence of some one-way (asymmetric) perturbation along the chain. According to this perspective, these modes should not split by any complicated deformation of the PA structure. This tendency will be magnified in the PA with a larger number of rods, because such a PA—when we focus on its local part—is equivalent to an isolated string of 1D array: no mode-splittings would occur particularly in the extremely large PA (with the infinite number of rods). The PA with a smaller number of rods, on the other hand, will lift the mode degeneracy more easily by the shape modification, since such a PA can no more be regarded as an isolated string of 1D array for the smallness of the whole PA. Actually, we confirmed that the mode splitting $\Delta\omega$ is a rapidly decreasing function of the rod number N: we obtained 0.0097, 0.0060, and 0.0036 for N=10, 20, and 50, respectively, for, e.g., mode 1 at e=0.776. We thus recognize that it is important to take into account the q1D feature of the closed PA structure as well as to consider it from the group-theoretic standpoint. This presents a great contrast to the similar phenomena for the modes in the 2D or 3D structures, for which the group-theoretic considerations would suffice. Next, we would like to refer to the unusual $\Delta\omega - n$ relation in Fig. 4. It is interesting to note that this n-dependence of $\Delta\omega$ is very different from the Stark effect [23] of the Hydrogen atom for which the splitting width varies simply like $\Delta\omega \propto n^2$. For the modes of smaller n, light is loosely bound around the PA because of their shorter lifetime, which ought to render its intensity distributions more sensitive to the PA modification. The modes near the band edge, on the other hand, have the lifetime that is barely retained very long in a fixed (symmetric) PA structure. This implies that their life is vulnerable even to a slight perturbation to the structure and hence its abrupt reduction may cause marked splittings of degenerate modes.

As mentioned on the light field distributions in Sec. 4.2, the structurally deformed PAs have a variety of optical responses. In particular, the band-edge modes (e.g., modes 9H and 9L) exhibit a strong anisotropy of excitation. Moreover, it should be emphasized that this anisotropy is very sensitive to the modification of the structure, i.e., it occurs even under a slight modification of the structure. This implies that optical excitations can be controlled by the mechanical deformation of the structure, which could have a potential to be exploited as high-function devices such as opto-mechanical devices [28]. We therefore believe that the present results will find a number of valuable applications as very high-Q resonators in the state-of-the-art technologies for the optical information systems, which combine the mechanical forces, the electronic phenomena, and the optical processes.

5. Laser oscillations

Because of the scaling rule that holds in our calculation in a similar manner to in the PCs, ω, τ and $K_a^{''}$ values normalized in the units of $2\pi c/L$, L/c and $2\pi/L$ respectively are determined by f (neither d nor L). We here use the ω, τ and $K_a^{''}$ values thus normalized.

http://dx.doi.org/10.5772/53435

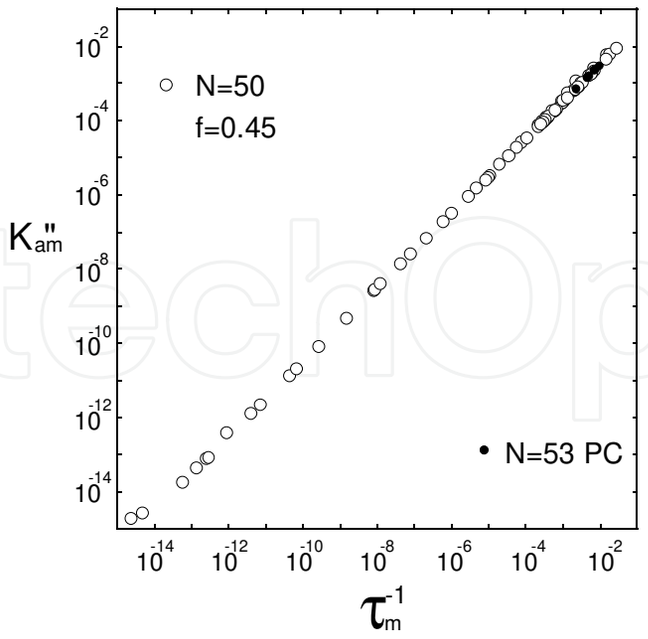

Figure 10. Relation between the threshold amplitude gain K''_{am} and the inverse photon-lifetime τ_m^{-1} for lasing modes. K''_{am} and τ_m are normalized in the units of $2\pi / L$ and L / c, respectively. The closed circles show the results for the band-edge modes near the top of the first band of the 2D PC resonator with 53 rods made of the same material as the rods in the present atoll structure (GaAs). See also Sections 2.2 and 2.3.

We studied the characteristics of a photonic atoll as a laser oscillator by assuming that every rod has the same optical amplitude gain K_a''. The method mentioned in Sec. 2.3 determines the threshold amplitude gain K_{am}'' for laser oscillation. In this calculation, we did not take into account absorption and other possible losses in order to isolate the effects inherent to the resonator's geometry. Some modes did not laser-oscillate even when K_a'' was very high (they were shown in Fig. 1 by dotted lines, see also Sec. 2.3). Here, we therefore consider only lasing modes (solid lines in Fig. 1). Figure 10 shows the relation between the threshold amplitude gain K_{am}'' thus obtained and the inverse lifetime τ_m^{-1} for lasing modes. These points are seen to line up with a slope of 45 on a log-log plot. The inverse proportionality between K_{am}'' and τ_m values is reasonable since the increased photon lifetime makes light stay in the resonator for a longer time and drives the laser to oscillate at lower optical gain. Figure 10 may be the first numerical verification of this kind of relation for the photonic-atoll resonator made of closed array of rods, though this kind of relation was also shown for a simple 1D resonator comprising a uniform medium sandwiched between two clear-cut mirrors [4]. The closed circles in this figure also show the results for the band-edge modes near the top of the first band of a 2D PC made of 53 GaAs rods [6]. When we compare the results from the two structures, the threshold gain values obtained for the PC are pessimistically higher than those for the atoll. In other words, laser oscillations with extremely low thresholds can be obtained by using our atoll structures. Noteworthy here is that the two resonators lead to very different results despite the fact that they contain a similar number

of rods and that extended modes are responsible for laser oscillations in both resonators. These results again confirm the superiority of the present structure over other PC-based structures.

6. Conclusion

We have theoretically demonstrated that very high *Q* factors and resultant very long photon lifetimes can be achieved by using the closed periodic array of microstructures, which we call a photonic-atoll (PA) resonator. Although other possible losses of light remain to be considered before this structure is put to practical use, the results we obtained suggest that it would be an excellent structure for confining light. In particular, the fact that it does not require a large size to achieve a strong light confinement will prove a great advantage over other ways of light confinement when it is incorporated into optical integrated circuits. Through the investigation for the PAs with a variety of elliptical forms, we found that the photon lifetime is maximized for the symmetric (or circular) form of the resonator. This structure deformation was also shown to give rise to the degeneracy lifting for eigen modes: even a slight deformation created pronounced splitting widths especially for the near-Γ-point modes and the near-band-edge modes whereas it did not for the modes in the middle of the band. Moreover, the band-edge modes split were found to exhibit a striking anisotropy of excitations, while other modes did not show any pronounced anisotropy. These mode splittings should be discussed taking into account the q1D-dimensionality of the structure as well as considering it from the group-theoretic standpoint. We have thus clarified the metamorphoses of the eigen modes split by the modification of the PA structures. Finally, we demonstrated the PA-laser oscillations with very low thresholds, which are much lower than those for the PC band edge lasers. These results would provide much information to understand the relevant resonators more deeply, which we believe will also be possibly exploited as a very high-*Q* resonator in the future optical information processing systems.

Author details

S. Nojima

Department of Nanosystem Science, Graduate School of Nanobioscience, Yokohama City University, Kanazawa, Yokohama, Kanagawa, Japan

References

[1] O. Painter O., Lee RK., Scherer A., Yariv A., O'Brien JD., Dapkus PD., Kim I., Science 1999; 284, 1819.

[2] Chang RK., Campillo AJ., editor. Optical Processes in Microcavities: World Scientific; 1996.

[3] Berman P., editor. Cavity Quantum Electrodynamics: Academic Press; 1994.

[4] Marcuse D., Principles of Quantum Electronics: Academic Press; 1980.

[5] Nojima S., Jpn. J. Appl. Phys. 1998; 37, L565.

[6] Nojima S., J. Appl. Phys. 2005; 98, 043102.

[7] Nojima S., Appl. Phys. Lett. 2001; 79, 1959.

[8] Vučković J., Lončar M., Nabuchi H., Scherer A., Phys. Rev. E 2001; 65, 016608.

[9] Ryu HY., Kim SH., Park HG., Hwang JK., Lee YH., Kim JS., Appl. Phys. Lett. 2002; 80, 3883.

[10] Happ TD., Tartakovskii II., Kulakovskii VD., Reithmaier JP., Kamp M., Forchel A., Phys. Rev. B 2002; 66, 041303.

[11] Akahane Y., Asano T., Song BS., and Noda S., Nature 2003; 425, 944.

[12] Nojima S., Nakahata M., J. Appl. Phys. 2009; 106, 043108.

[13] Nojima S., Yawata M., J. Phys. Soc. Jpn. 2010; 79, 043401.

[14] Takeda MW., Kirihara S., Miyamoto Y., Sakoda K., Honda K., Phys. Rev. Lett. 2004; 92, 093902.

[15] Lin HB., Eversole JD., Campillo AJ., J. Opt. Soc. Am. B 1992; 9, 43.

[16] Gayral B., Gérard JM., Lemaître A., Dupuis C., Manin L., Pelouard JL., Appl. Phys. Lett. 1999; 75, 1908.

[17] Moon HJ., Chough YT., and An K., Phys. Rev. Lett. 2000; 85, 3161.

[18] Armani DK., KippenbergTJ., Spillane SM., Vahala KJ., Nature 2003; 421, 925.

[19] Gmachl C., Capasso F., Narimanov EE., Nöckel JU., Stone AD., Faist J., Sivco DL., Cho AY., Nature1998; 280, 1556.

[20] Nojima S., J. Phys. Soc. Jpn. 2007; 76, 023401.

[21] Nojima S., Phys. Rev. B 2002; 65, 073103.

[22] Nojima S., J. Phys. Soc. Jpn. 2005; 74, 577.

[23] Landau LD., Lifshitz EM., Quantum Mechanics: Non-relativistic Theory: Butterworth-Heinemann; 1981.

[24] Post EJ.,Rev. Mod. Phys. 1967; 39, 475.

[25] Abramowitz M., Stegun IA., Handbook of Mathematical Functions: Dover; 1972.

[26] Villeneuve P R and Piché M, Phys. Rev. B 1992; 46, 4969.

[27] Nojima S., Usuki M., Yawata M., Nakahata M., Phys. Rev. A 2012; 85, 063818.

[28] Eichenfield M., Chan J., Camacho RM., Vahala KJ., Painter O., Nature 2009; 462, 78.

IntechOpen